CHEMISTRY OF MATERIALS
Article

Chem. Mater. **2011,** *23,* 1061–1069 1061
DOI:10.1021/cm103326n

Enhanced Thin-Film Transistor Performance by Combining 13,6-N-Sulfinylacetamidopentacene with Printed PEDOT:PSS Electrodes

Alessandro Luzio,[†] Chiara Musumeci,[‡] Christopher R. Newman,[§] Antonio Facchetti,*[,§] Tobin J. Marks,*[,§] and Bruno Pignataro*[,∥]

[†]*Dipartimento di Ingegneria Industriale, Università di Palermo, V.le delle Scienze, Parco D'Orleans II - 90128 Palermo − Italy,* [‡]*Superlab-Consorzio Catania Ricerche, Stradale Primosole 50, 95121, Catania − Italy,* [§]*Department of Chemistry and the Materials Research Center, Northwestern University, 2145 Sheridan Road, Evanston, Illinois 60208, United States and Polyera Corporation 8045 Lamon Avenue, Skokie, Illinois 60077, United States , and* [∥]*Dipartimento di Chimica "S. Cannizzaro", Università di Palermo, V.le delle Scienze, Parco D'Orleans II - 90128 Palermo − Italy*

Received November 19, 2010. Revised Manuscript Received December 22, 2010

Bottom-contact/bottom-gate organic thin-film transistors (OTFTs) are fabricated using a soluble pentacene precursor (13,6-*N*-sulfinylacetamidopentacene; SAP) and inkjet printed PEDOT:PSS electrodes on bare SiO_2 dielectrics. Saturation mobility, I_{on}/I_{off} ratio, and threshold voltage parameters, respectively, of 0.27 $cm^2 V^{-1} s^{-1}$, 10^5, and −4.25 V were measured under ambient conditions after the thermal conversion of SAP to pentacene in 100 μm long channel OTFT devices. The results obtained by the above solution approach are comparable to that of vapor-phase grown pentacene-based OTFTs with photolithographic gold contacts and organic buffer layers and/or inorganic injection layers. The present high performance level is ascribed to the morphological continuity and uniformity of the first few layers of the polycrystalline semiconductor phase at the interface with the organic electrodes, which in effect constitute an ideal chemical interface for the converted SAP. In contrast, gold electrodes thermally evaporated by employing shadow masks result in blurred-edge regions, drastically affecting the semiconductor morphology along with the transport properties.

1. Introduction

During the past two decades, the implementation of molecular organic semiconductors in electronics has offered great potential for emerging technologies such as nanoelectronics, organic electronics, and plastic electronics.[1−3] In particular, great attention has been devoted to the development of organic thin-film transistors (OTFTs) since these are promising candidates as active elements in numerous types of switching devices, smart cards,[1,4] sensors, and biosensors,[5] to cite just a few applications. In this respect, diverse varieties of organic semiconductors including both conjugated polymers and small molecules have been employed.[6,7] Among these systems, vacuum-sublimed pentacene TFTs exhibit impressive performance, surpassing that of hydrogenated amorphous silicon.[8] Unfortunately, pentacene is insoluble in most organic solvents, thus hindering implementation in printed transistors and circuits. However, solution approaches based on soluble pentacene precursors and 9,10-functionalized pentacenes may open avenues to the practical use of this material.[8−10]

In addition to the above pentacene functionalization efforts, impressive studies have reported the synthesis and/or exploitation of pentacene derivatives designed to improve both solubility and charge transport by increasing solid state intermolecular π-orbital overlap.[11] Thus, 6,13-bis(triisopropylsilylethynyl) pentacene (TIPS-PEN) exhibits mobility > 1 $cm^2 V^{-1} s^{-1}$, current on/off ratios > 10^8, and threshold voltages ∼0−10 V.[12] Other studies reported the thermal or photoconversion of Diels−Alder pentacene precursors,[13−18] including 13,6-*N*-sulfinylacetamidopentacene (SAP) which has been used to fabricate medium (15 μm)[13] and short (40−100 nm)[19] channel length OTFTs,

*Corresponding author e-mail: a-facchetti@northwestern.edu (A.F.); t-marks@northwestern.edu (T.J.M.); bruno.pignataro@unipa.it (B.P.).

(1) Whitesides, G. M.; Lipomi, D. J. *Faraday Discuss.* **2009**, *143*, 373.
(2) Di Benedetto, S. A.; Facchetti, A.; Ratner, M. A.; Marks, T. J. *Adv. Mater.* **2009**, *21*, 1407.
(3) Rogers, J. A.; Someya, T.; Huang, Y. *Science* **2010**, *327*, 1603.
(4) Zaumseil, J.; Sirringhaus, H. *Chem. Rev.* **2007**, *107*, 1296.
(5) Sokolov, A. N.; Roberts, M. E.; Bao, Z. *Mater. Today* **2009**, *12*, 09.
(6) Tanese, M. C.; Farinola, G. M.; Pignataro, B.; Valli, L.; Giotta, L.; Conoci, S.; Lang, P.; Colangiuli, D.; Babudri, F.; Naso, F.; Sabbatici, L.; Zambonin, P. G.; Torsi, L. *Chem. Mater.* **2006**, *18*, 778.
(7) Tanese, M. C.; Pignataro, B.; Farinola, G. M.; Colangiuli, D.; Valli, L.; Giotta, L.; Conoci, S.; Marinelli, F.; Babudri, F.; Naso, F.; Sabbatini, L.; Zambonin, P. G.; Torsi, L. *Thin Solid Films* **2008**, *516*, 3263.
(8) Anthony, J. E. *Angew. Chem., Int. Ed.* **2008**, *47*, 452.
(9) Facchetti, A. *Mater. Today* **2007**, *10*, 28.
(10) Allard, S.; Forster, M.; Souharce, B.; Thiem, H.; Scherf, U. *Angew. Chem., Int. Ed.* **2008**, *47*, 4070.
(11) Anthony, J. E.; Eaton, D. L.; Parkin, S. R. *Org. Lett.* **2002**, *4*, 15.
(12) Park, S. K.; Anthony, J. E.; Mourey, D. A.; Jackson, T. N. *Appl. Phys. Lett.* **2007**, *91*, 063514.
(13) Afzali, A.; Dimitrakopoulos, C. D.; Breen, T. L. *J. Am. Chem. Soc.* **2002**, *124*, 8812.
(14) Afzali, A.; Dimitrakopoulos, C. D.; Graham, T. O. *Adv. Mater.* **2003**, *15*, 2066.

Published on Web 01/10/2011

exhibiting mobilities as high as 0.42 $cm^2\ V^{-1}\ s^{-1}$ and 0.022 $cm^2\ V^{-1}\ s^{-1}$, respectively.

A critical issue affecting OTFT performance is the contact resistance, which depends on the device architecture and the chemical compatibility between the source/drain (S/D) electrodes and the organic semiconductor. As to the device architecture, both top-contact and bottom-contact devices have been investigated using evaporated pentacene and gold S/D electrodes. Although the bottom-contact arrangement is attractive for manufacturing subtenth μm channel lengths,[20] the top-contact configuration is generally preferred for research measurements due to its ease of fabrication. As a matter of fact, in many studies a fall in mobility to about $10^{-3}\ cm^2/(V\ s)$ in pentacene-based devices has been ascribed to the change from a top to bottom-contact configuration.[20−24] In other reports, a multistep process has been used to realize S/D electrodes in a bottom-contact configuration, i.e., by introducing gold deposition, photolithography, and lift-off patterning, and the resulting pentacene mobilities are comparable to the best reported in the literature.[25]

Thus, it is clear that the S/D electrode resolution plays an important role in the bottom-contact configuration, and the use of shadow masks in a single step patterning process may result in low performance.[21] This fact has been related to strong gold surface effects on the pentacene nucleation and growth, leading to non-uniform film microstructure on the S/D electrode surfaces.[23,24] However, as long as high S/D pattern resolution is maintained, this has negligible effect on the measured mobility, although it still affects the contact resistance.[23] Nevertheless, low resolution patterning, leading to significant gold contamination in the channel, in proximity to the contacts, can dramatically influence the pentacene growth morphology.[21]

To prevent the growth of "low-mobility semiconductor regions" either on the top of metallic OTFT electrodes or in their proximity, modification of the metal surface by self-assembled monolayers (SAMs),[20,22,26,27] by chemical[28,29] or plasma[30,31] treatments, or by electrochemically deposited poly(3,4-ethylenedioxythiophene):poly(styrenesulfonate) (PEDOT:PSS)[32] has been investigated. However, all of these approaches may also affect the structure of the channel region. For these reasons, printing techniques are promising for selectively coating or replacing gold electrodes by conductive polymers such as PEDOT:PSS. Moreover, inkjet printing of S/D electrodes represents a single-step additive process of great value for realizing large-area, low-cost devices.

The compatibility of printed PEDOT:PSS S/D contacts with evaporated pentacene has been investigated, yielding bottom-contact OTFT performance comparable to that of top-contact devices.[33,34] Furthermore, top-contact devices with PEDOT:PSS S/D electrodes exhibit enhanced performance versus comparable devices fabricated with gold electrodes.[35] Nevertheless, despite these promising results, no studies have addressed the intriguing prospect of combining a solution-processable pentacene with solution-processable PEDOT:PSS electrodes in OTFTs, information necessary to advance to OTFTs in which all components are printed.

As a promising soluble pentacene precursor, SAP has been studied in conventional[13] and hybrid OTFTs with channel lengths varied from submicrometer to 100 μm.[36−41] Recently, Tulevski et al. studied contact resistance effects in SAP-based OTFTs,[19] reporting decreased contact resistance in submicrometer channels by gold electrode derivatization with thioketone SAMs. Note that when the device dimensions are greatly reduced, the electrode-semiconductor contact resistance exceeds the channel resistance and dominates the OTFT response. However, this regime applies mainly to single pentacene grain electronic characteristics and not to the polycrystalline microstructure arising from SAP conversion.

Here we report on high-performance bottom-contact 100 μm channel OTFTs fabricated with a pentacene active layer obtained by the thermal conversion of solution-processed SAP that, for the first time, is coupled with inkjet printed PEDOT:PSS S/D electrodes. This approach is shown to be an effective and low cost means

(15) Brown, A. R.; Pomp, A.; deLeeuw, D. M.; Klaassen, D. B.; Havinga, E. E. M.; Herwig, P.; Müllen, K. J. *Appl. Phys.* **1996**, *79*, 2136.
(16) Herwig, P. T.; Müllen, K. *Adv. Mater.* **1999**, *11*, 480.
(17) Mitzi, D. B.; Afzali, A. *Cryst. Growth Des.* **2007**, *7*, 691.
(18) Weidkamp, K. P.; Afzali, A.; Tromp, R. M.; Hamers, R. J. *J. Am. Chem. Soc.* **2004**, *126*, 12740.
(19) Tulevski, G. S.; Miao, Q.; Afzali, A.; Graham, T. O.; Kagan, C. R.; Nuckolls, C. *J. Am. Chem. Soc.* **2006**, *128*, 1788.
(20) Kymissis, I.; Dimitrakopoulos, C. D.; Purushothaman, S. *IEEE Trans. Electron Devices* **2001**, *48*, 1060.
(21) Noda, M.; Yoneya, N.; Hirai, N.; Kawashima, N.; Nomoto, K. *Mater. Res. Soc. Symp. Proc.* **2004**, *814*, I4.4.1.
(22) Gundlach, D. J.; Jia, L.; Jackson, T. N. *IEEE Trans. Dev. Lett.* **2001**, *22*, 571.
(23) Gupta, D.; Katiyar, M.; Gupta, D. *Org. Electron.* **2009**, *10*, 775.
(24) Hong, K.; Yoon Yang, S.; Yang, C.; Kim, S. H.; Choi, D.; Park, C. E. *Org. Electron.* **2008**, *9*, 864.
(25) Kumaki, D.; Umeda, T.; Tokito, S. *Appl. Phys. Lett.* **2008**, *92*, 013301.
(26) Ihm, K.; Kim, B.; Kang, T.; Kim, K.; Joo, M. H.; Kim, T. H.; Yoon, S. S.; Chung, S. *Appl. Phys. Lett.* **2006**, *89*, 033504.
(27) Hamadani, B. H.; Corley, D. A.; Ciszek, J. W.; Tour, J. M.; Natelson, D. *Nano Lett.* **2006**, *6*, 1303.
(28) Di, C.; Yu, G.; Liu, Y.; Xu, X.; Wei, D.; Song, Y.; Sun, Y.; Wang, Y.; Zhu, D.; Liu, J.; Liu, X.; Wu, D. *J. Am. Chem. Soc.* **2006**, *128*, 16418.
(29) Maeda, T.; Kato, H.; Kawakami, H. *Appl. Phys. Lett.* **2006**, *89*, 123508.
(30) Kim, W.; Hong, K.; Lee, J. L. *Appl. Phys. Lett.* **2006**, *89*, 142117.
(31) Lee, H. S.; Cho, J. H.; Kim, W.-K.; Lee, J.-L.; Cho, K. *Electrochem. Solid-State Lett.* **2007**, *10*, H239.
(32) Schroeder, R.; Majewski, L. A.; Grell, M.; Maunoury, J.; Gautrot, J.; Hodge, P.; Turner, M. *Appl. Phys. Lett.* **2005**, *87*, 113501.
(33) Halik, M.; Klauk, H.; Zschieschang, U.; Schmid, G.; Radlik, W.; Weber, W. *Adv. Mater.* **2002**, *14*, 1717.
(34) Hong, K.; Yang, S. Y.; Yang, C.; Kim, S. H.; Choi, D.; Park, C. E. *Org. Electron.* **2008**, *9*, 864.
(35) Li, D.; Guo, L. J. *Appl. Phys. Lett.* **2006**, *88*, 063513.
(36) Volkman, S. K.; Molesa, S.; Mattis, B.; Chang, P. C.; Subramanian, V. *Mater. Res. Soc. Symp. Proc.* **2003**, *769*, H11.7.1/L12.7.1.
(37) Molesa, S. E.; de la Fuente Vornbrock, A.; Chang, P. C.; Subramanian, V. In *Electron Devices Meeting*, IEDM Technical Digest. IEEE International: 2005; p 109.
(38) Kagan, C. R.; Afzali, A.; Graham, T. O. *Appl. Phys. Lett.* **2005**, *86*, 193505.
(39) Akinaga, T.; Yasutake, S.; Sasaki, S.; Sakata, O.; Otsuka, H.; Takahara, A. *Chem. Lett.* **2006**, *35*, 1162.
(40) Wang, X.; Ochiai, S.; Kojima, K.; Ohashi, A.; Mizutani, T. *J. Vac. Soc. Jpn.* **2008**, *51*(3), 169.
(41) Orecchini, G.; Zhang, R.; Agar, J.; Staiculescu, D.; Tentzeris, M. M.; Roselli, L.; Wong, C. P. Electronic Components and Technology Conference (ECTC), Proceedings 60th **2010**; p 985.

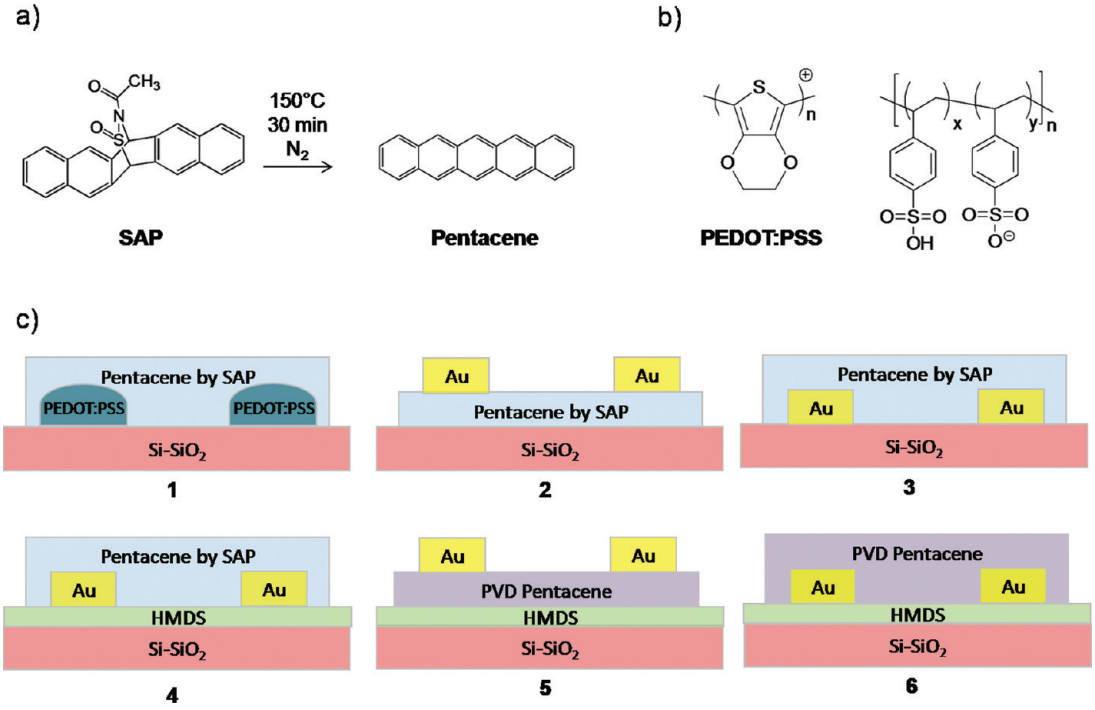

Figure 1. a) SAP retro Diels−Alder conversion to pentacene. b) Molecular structure of PEDOT:PSS. c) Schematic representation of the OTFTs used in this study employing a bottom gate configuration and Si-SiO_2 substrates: pentacene by SAP thermal conversion in bottom/PEDOT:PSS (device **1**), top/Au (device **2**), and bottom/Au (device **3**) S/D geometries; the same structure of device **3** but with an HMDS-treated dielectric surface (device **4**); thermally evaporated pentacene in bottom/Au (device **5**) and top/Au (device **6**) S/D geometries with an HMDS-treated gate dielectric.

to reduce the contact resistance. We focus on understanding the important role of the contact interfaces, and we compare/contrast the microstructural properties of the above devices with those employing thermally evaporated gold electrodes.

2. Experimental Section

Figure 1 summarizes the materials and the device architectures employed here. Pentacene active layers were obtained by thermal conversion (retro Diels−Alder reaction) of 13,6-*N*-sulfinylacetamido pentacene (SAP, Sigma−Aldrich, 97%; devices **1**-**4**). SAP was dissolved in dry chloroform to achieve concentrations of ~20 mg/mL. Heavily p-doped Si wafers with 300 nm thermally grown oxide (Si/SiO_2) served, respectively, as the gate electrode and the gate dielectric for the OTFTs. To minimize charge trapping effects, the SiO_2 surfaces of some devices were functionalized with 1,1,1,3,3,3-hexamethyldisilazane (HMDS; Sigma−Aldrich) by prolonged exposure to HMDS-saturated vapor, leading to a dense Si-CH_3 surface coverage (devices **4**-**6**). Advancing contact angles $>90°$ were measured by employing water microdroplets on these surfaces and are consistent with the extensive surface silylation (bare SiO_2 showed a contact angle of ~50°).

Inkjet printing of the S/D electrodes (device **1**) was performed using an aqueous dispersion of poly(3,4-ethylene dioxythiophene) poly(styrenesulfonate) (PEDOT:PSS; 1.3 wt.% dispersion in H_2O; Sigma-Aldrich). A properly formulated suspension enables jetting of the ink along with good control of pattern and printing resolution. Thus, the aqueous PEDOT:PSS dispersion was further diluted with DI water to 0.43 wt.%. Either ethylene glycol or glycerol (20% V/V) was added to the ink to avoid clogging of the cartridge nozzles and spreading of the ink over the nozzle surface, exploiting the polyol humectant and plasticizer tendencies.[42] Both glycerol and ethylene glycol are known to significantly increase PEDOT:PSS film conductivity.[43] The conductive ink was filtered through a 0.2 μm hydrophilic filter just before printing. To avoid contamination of the channel (flying and satellite drops, volume fluctuations, tail formation), the jetting voltage was sequentially tuned between 25 and 40 V by controlling the droplet shape with a camera. To avoid unwanted phenomena such as dewetting, pinning, and coalescence, a plate temperature of 70 °C, a cartridge temperature of 35 °C, and a multilayer printing procedure were employed. Accordingly, 6−12 layers were deposited with an interlayer delay of 60 s, and a drop spacing varied between 40-80 μm. Evaporation of residual solvent was carried out in a vacuum oven at 110 °C for 1 h. Using this procedure, channels with 40-100 μm lengths and PEDOT:PSS electrode conductivities as high as 140 S/cm are realized. For gold S/D electrodes (devices **2**−**6**), 30 nm thick contacts were obtained by thermal evaporation (PVD) with a Denton Vacuum Explorer thermal deposition system, assisted by a SQC-122c controller. Chloroform solutions of 13,6-N-sulfinylacetamidopentacene were drop-cast or spun on bare oxide substrates at 1500 rpm for 1 min using a Laurell WS − 400B − 6NPP/LITE spin coater and were then dried on a hot plate for 3 min at 80 °C. SAP conversion to semiconducting pentacene was achieved under N_2 at 150 °C for 30 min. In addition, 40 nm thick thermal vapor-deposited pentacene (sublimed grade, ≥99.9% pure trace metals basis; Sigma-Aldrich) was also used as the active phase for comparative studies (devices **5** and **6**; growth parameters: 60 °C, 0.1 Å/s).

OTFT electrical measurements were performed under ambient atmosphere. I−V curves, transfer characteristics, and output

(42) Tan, L.; Kong, Y. P.; Pang, S. W.; Yee, A. F. *J. Vac. Sci. Technol., B: Microelectron. Nanometer Struct.--Process., Meas., Phenom.* **2004**, *22*, 2486.

(43) Ouyang, J.; Xu, Q.; Chu, C.; Yang, Y.; Li, G.; Shinar, J. *Polymer* **2004**, *45*, 8443.

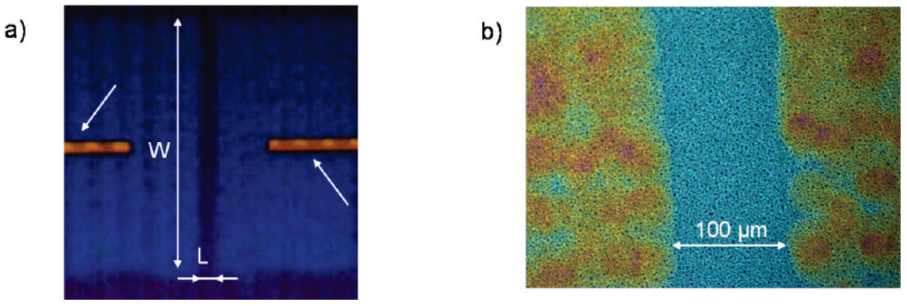

Figure 2. Optical micrographs of a) an inkjet printed PEDOT:PSS channel (L = 100 μm; W = 1000 μm). The arrows mark the gold lead contacts; b) the same device after SAP deposition and its thermal conversion to pentacene.

plots were obtained by employing a 4-probe probe station interfaced to a Keithley 6340 subfemtoamp meter and a Keithley 2400 source meter. A Veeco profilometer was used for film thickness measurements. Film microstructure and morphology were investigated by X-ray diffraction (WAXRD; Rigaku, CuKα monochromic radiation) and tapping-mode AFM (Veeco Digital Instrument MultiMode SPM). For AFM, commercially available etched-Si probes with a pyramidal-shaped tips having a nominal curvature of 10 nm and a nominal internal angle of 35° were used. During scanning, the 125 μm-long cantilever, with a nominal spring constant in the range of 20−100 N/m, oscillated at its resonance frequency of ∼330 kHz. Height and phase images were collected by capturing 512 × 512 points in each scan, and the scan rate was maintained below 1 line/s. During imaging, temperature and humidity were ∼298 K and ∼40%, respectively.

3. Results and Discussion

3.1. Pentacene Thin Film Transistor Characterization. Figure 2 shows optical micrographs of a representative bottom-contact OTFT realized using converted SAP as the semiconductor and inkjet printed PEDOT:PSS S/D electrodes. Figure 2a shows the structure of a device with an average electrode thickness of ∼40 nm, channel length of ∼100 μm, and channel width of ∼1.0 mm (device **1**). Gold leads for facile engagement with the source-meter unit are also shown. Figure 2b depicts the optical image on the same device after SAP film deposition and thermal conversion to pentacene. After OTFT fabrication, the response characteristics of devices **1** were measured in air. OTFT performance parameters, including field-effect mobility (μ) and threshold voltage (V_T), were extracted from the transfer characteristics of the transistors. In the saturation regime, the drain-source current (I_{DS}) is expressed as follows[44]

$$I_{DS} = W \cdot C_i/(2 \cdot L) \cdot \mu_{sat} \cdot (V_G\text{-}V_T)^2 \qquad (1)$$

where W and L are, respectively, the channel width and the channel length, C_i is the capacitance per unit area of the gate insulator, and V_G is the gate voltage. Figure 3 shows the transfer (Figure 3a) and output (Figure 3b) characteristics of a typical device **1**. From the $(I_{DS})^{1/2}$ vs V_G fit to eq 1, a straight line with the slope proportional to the field effect mobility is obtained, as an indication of the well-behaved response of this device. By fitting the data in the saturation regime to eq 1, μ_{sat} = 0.27 cm^2 V^{-1} s^{-1} and V_T = −4.25 V are obtained, with I_{on}/I_{off} ∼10^5. From the subthreshold regime data, the observed subthreshold slope (SS) in proximity to the onset is ∼5 V/dec, whereas 12 V/dec is obtained close to the threshold voltage.

Although our study is centered on the electrode/semiconductor organic interface, we believe that the observed device behavior could be further improved by limiting the observed leakage currents (see Figure 3b). Several papers report on possible methods to reduce leakages and further studies are needed also in view of realizing fully organic devices with high-quality dielectrics.[45] More interestingly, by analyzing the transfer characteristics, it can be seen that this device exhibits a positive V_{on} of ∼10 V. Numerical simulations indicate that this type of onset shift is caused by acceptor-like states deep in the bandgap.[46,47] Several studies show that such acceptor-like states are frequently induced by O_2 and/or water incorporation in the organic semiconductor films.[48] Moreover, in some pentacene films, this behavior appears to result from nonuniform doping, with O_2 incorporated in areas of low structural order, and dependent on the film and contact morphology.[49] Also, the PEDOT:PSS morphology could conceivably affect the aforementioned acceptor-like states, since previous studies demonstrated a vertical segregation of PSS at the top layer, and thus a PSS protonation doping mechanism at the PSS/pentacene interface may be expected.[50] This is also in agreement with recent experiments employing a PEDOT:PSS/poly(9,9-dihexylfluorene) (PF) or a PEDOT:PSS/poly(9,9-dioctyl-fluorene-cobithiophene) (F8T2) contact layer acting as an electron trapping surface, which favors the accumulation of negative charges and thereby the presence of an additional electric field at the interface.[51,52]

(44) Horowitz, G. *J. Mater. Chem.* **1999**, *9*, 2021.
(45) Facchetti, A.; Yoon, M. H.; Marks, T. J. *Adv. Mater.* **2005**, *17*, 1705.
(46) Scheinert, S.; Paasch, G.; Doll, T. *Synth. Met.* **2003**, *139*, 233.
(47) Volkel, A. R.; Street, R. A.; Knipp, D. *Phys. Rev. B* **2002**, *66*, 195336.
(48) Meijer, E. J.; Detcheverry, C.; Baesjou, P. J.; van Veenendaal, E.; de Leeuw, D. M.; Klapwijk, T. M. *J. Appl. Phys.* **2003**, *93*, 4831.
(49) Knipp, D.; Muck, T.; Benor, A.; Wagner, V. *J. Non-Cryst. Solids* **2006**, *352*, 1774.
(50) Timpanaro, S.; Kemerink, M.; Touwslager, F. J.; De Kok, M. M.; Schrader, S. *Chem. Phys. Lett.* **2004**, *394*, 339.
(51) Kanaan, H.; Jolinat, P.; Ablart, G.; Destruel, P.; Renaud, C.; Lee, C. W.; Nguyen, T.-P. *Org. Electron.* **2010**, *11*(6), 1047.
(52) Wang, J. Z.; Chang, J. F.; Sirringhaus, H. *Appl. Phys. Lett.* **2005**, *87*, 083503.

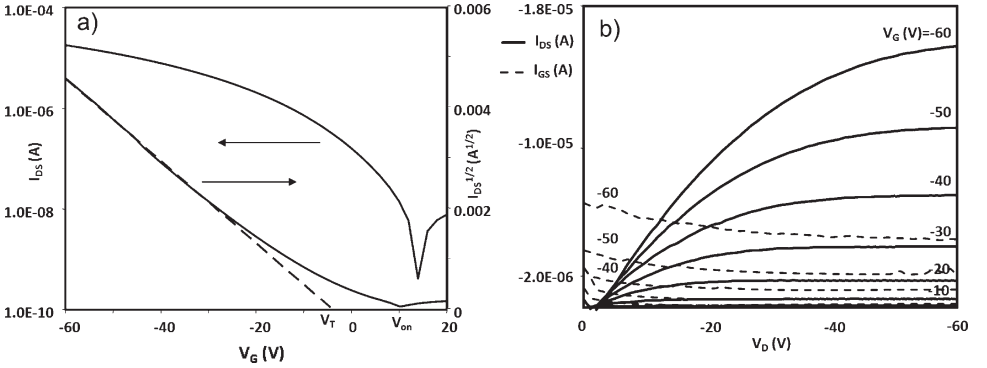

Figure 3. Transfer (a) and output (b) curves of OTFT employing SAP-derived pentacene and inkjet printed PEDOT:PSS source and drain electrodes (device **1**). Leakage currents are reported at the different V_G values by the dashed lines in 3b.

Table 1. Pentacene OTFT Performance Data As a Function of Film-Contact Characteristics

device	pentacene deposition method	S/D material	S/D configuration	dielectric	mobility ($cm^2 V^{-1} s^{-1}$)	I_{on}/I_{off}	V_T (V)	SS (V/dec)
1	spin coating	PEDOT:PSS	bottom contact	SiO_2	0.27	10^5	−4.2	5
2	spin coating	Au	top contact	SiO_2	NO	NO	NO	NO
3	spin coating	Au	bottom contact	SiO_2	4×10^{-6}	10	32	NO
4	spin coating	Au	bottom contact	SiO_2/HMDS	0.0016	6.5×10^3	−24.6	9.5
5	PVD	Au	top contact	SiO_2/HMDS	0.328	2×10^6	−16.8	3
6	PVD	Au	bottom contact	SiO_2/HMDS	0.002	4×10^3	−24.3	8.5

OTFT performance data are summarized below in Table 1. For OTFTs fabricated from soluble pentacene derivatives, the device **1** results are important. As a reference, a device using spin-coated SAP converted to pentacene on HMDS-treated Si-SiO_2 substrates, having a channel length of 15 μm and width of 1500 μm, with electron-beam evaporated gold S/D electrodes, has been reported.[13] The authors showed μ_{sat} = 0.42 cm^2 V^{-1} s^{-1} and $I_{on}/I_{off} \sim 10^7$. Although V_T was not reported, analysis of the transfer characteristics of smaller channel devices (L = 4.8 μm, W = 1500 μm) allows derivation of a threshold voltage of −60/-70 V. Furthermore, long channel (95.6 μm) OTFTs using SAP-derived pentacene films, electron-beam evaporated gold S/Ds, and an HMDS-treated SiO_2 gate dielectric were also reported[38] and exhibit mobilities comparable to vacuum-deposited pentacene devices. However, no information on threshold voltages and the subthreshold regime behavior were provided. Therefore, devices **1** show mobility and I_{on}/I_{off} comparable to the best-performing SAP-derived OTFTs, with improved threshold voltages, despite the larger channels and untreated SiO_2 dielectric surfaces.

To rationalize the enhanced performance of these OTFTs, attempts were made to compare type **1** devices with those fabricated with converted SAP films and top gold contacts (type **2**). However, the latter devices are found to be inactive, presumably due to the poor injection characteristics of vapor-deposited gold on the rough converted pentacene surface (rms roughness ~150 nm), reflecting pentacene island formation (see Figure 5b below). Rough semiconductor surfaces depress effective metal-semiconductor contact area and reduce conductivity.[53]

(53) Knuyt, G.; Quaeyhaegens, C.; Haen, J. D.; Stals, L. M. *Phys. Status Solidi B* **1996**, *195*, 179.

In a different experiment, bottom-contact/bottom-gate OTFTs were fabricated in the device **1** configuration, but employing vapor-deposited gold S/D contacts patterned by using shadow masks during the deposition (device **3**). Interestingly, these devices are mostly inactive, and those that are active exhibit very poor performance with μ_{sat} = 4×10^{-6} cm^2 V^{-1} s^{-1}, V_T = 32 V, and I_{on}/I_{off} = 10. Note that the performance of the bottom-contact/bottom-gate devices with Au contacts is improved by treating the dielectric with HMDS (device **4**). For these OTFTs, the mobility increases by 1000× with respect to device **3**. Figure 4a shows the transfer characteristics, and Figure 4b the output of device **4** (L = 100 μm; W = 2000 μm), resulting in μ_{sat} = 0.0016 cm^2 V^{-1} s^{-1}, V_T = −24.6 V, and SS = 9.5 V/dec and $I_{on}/I_{off} \sim 6.5 \times 10^3$.

The poor performance of the gold contact devices likely reflects the microstructure of the converted pentacene films. Specifically, for PVD-derived pentacene films, a so-called "low mobility phase", i.e., a phase characterized by poor crystallinity and small grain size, has been observed either in proximity to, or on the top of, Au S/D electrodes.[23,24] The origin of this phase has been ascribed to the different molecular stacking of pentacene on the gold surface and to the consequent microstructural transition toward the channel. Moreover, a "blurred-edge" region of Au is formed due to lateral diffusion of Au particles at the edge of the shadow mask. This Au "contamination" enhances the extent of the low mobility phase in the channel, drastically affecting the pentacene transport properties.[21]

Informative comparisons can also be made by fabricating devices with vapor-deposited pentacene films, in top-contact (device **5**) and bottom-contact (device **6**) configurations, with the same deposition and patterning single step process for the Au S/D electrodes employed for devices **3** and **4**. In agreement with literature data,[21,24]

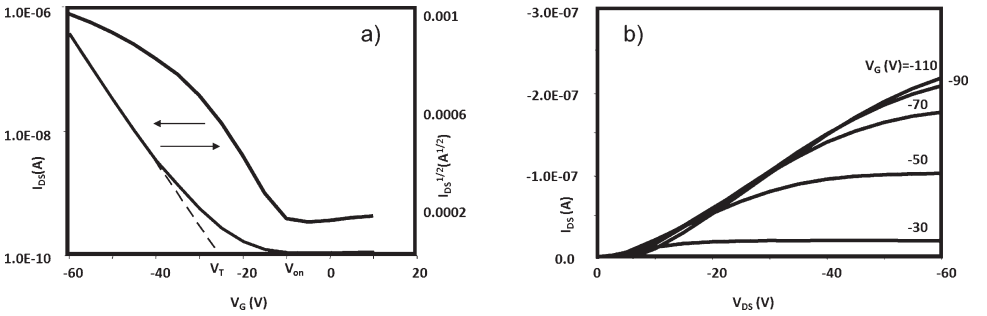

Figure 4. Transfer (a) and output (b) plots for OTFTs employing SAP-converted to pentacene and evaporated Au source and drain electrodes (device **4**).

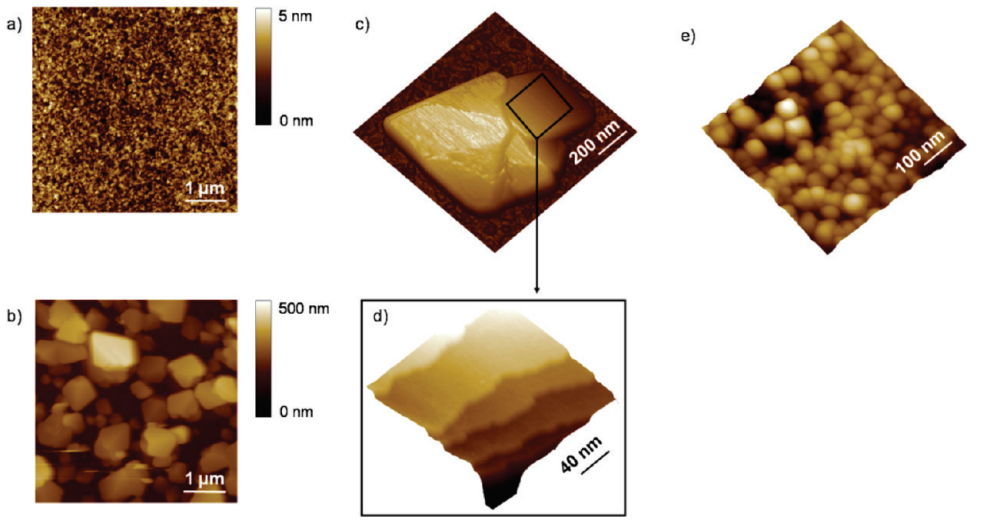

Figure 5. AFM images of a) SAP spin-coated on silicon dioxide; b) the corresponded film converted to pentacene at 150 °C for 30 min; c) a single island from image b) in a 3D view; d) expanded image of a selected region of image c); and e) the polycrystalline phase surrounding and/or underneath the islands. z scale: a) 5 nm; b) 500 nm; c) 1 μm; d) 20 nm; and e) 50 nm.

a 100× difference in mobility is observed between the two configurations (Table 1). These results allow us to reasonably ascribe the low mobility of pentacene in devices **3** and **4** to the same origin, i.e., the "low mobility region" in proximity to the electrodes. This interpretation is supported by the enhanced mobility achieved by using PEDOT:PSS electrodes (device **1**).

3.2. Microstructure of the Solution-Processed Semiconductor, Electrode Surfaces, and OTFT Performance. To understand how PEDOT:PSS electrodes enhance the OTFT performance of bottom-contact devices and to determine whether there are correlations with the semiconductor film microstructure, the morphological features of SAP-derived films were investigated. Figure 5 shows the AFM images of a SAP film spin-coated on Si/SiO_2 (Figure 5a), and the corresponding pentacene layer obtained after thermal conversion (Figure 5b). For a 160 nm thick film on Si/SiO_2, a rms roughness of 0.765 nm is extracted from the images, while after conversion, the pentacene films are characterized by a highly columnar growth mode leading to disconnected islands widely distributed in lateral size and up to 500 nm high (Figure 5b). Moreover, a continuous polycrystalline film structure surrounding and/or underneath the islands (Figure 5e) is also present. This phase has small grains (~20 nm wide), a rms roughness of ~5 nm, and a thickness of ~60 nm.

Out-of-plane wide-angle X-ray diffraction (WAXRD) measurements were performed on both precursor and converted films (Figure 6), revealing the amorphous nature of the precursor and the highly crystalline nature of the converted pentacene. Narrow peaks corresponding to the (00*l*) reflections of the pentacene "bulk phase"[54] are clearly visible. However, in contrast to PVD-derived pentacene films grown on SiO_2, the pentacene "thin film"[54] phase is not detected by WAXRD. This is consistent with WAXRD results from other groups suggesting the formation of typical terrace-like 3D crystal with the crystallographic *ab* plane parallel to the substrate surface.[54] Moreover, the in-plane GIXRD spectra exhibit (00*l*) reflection components, indicating tilting of the pentacene crystallographic *ab* plane with respect to the substrate surface, along with a disordered growth in the thin film phase.[39] Indeed, the AFM images (Figure 5d) confirm the terrace-like growth mode leading to pentacene islands, characterized by 1.5 nm step heights that are approximately one interplanar repeat distance in the pentacene "bulk phase".

Figure 7 below compares the AFM images of SAP-derived pentacene films on bare Si/SiO_2 (Figure 7a), on

(54) Ruiz, R.; Choudhary, D.; Nickel, B.; Toccoli, T.; Chang, K.-C.; Mayer, A. C.; Clancy, P.; Blakely, J. M.; Headrick, R. L.; Iannotta, S.; Malliaras, G. G. *Chem. Mater.* **2004**, *16*, 4497.

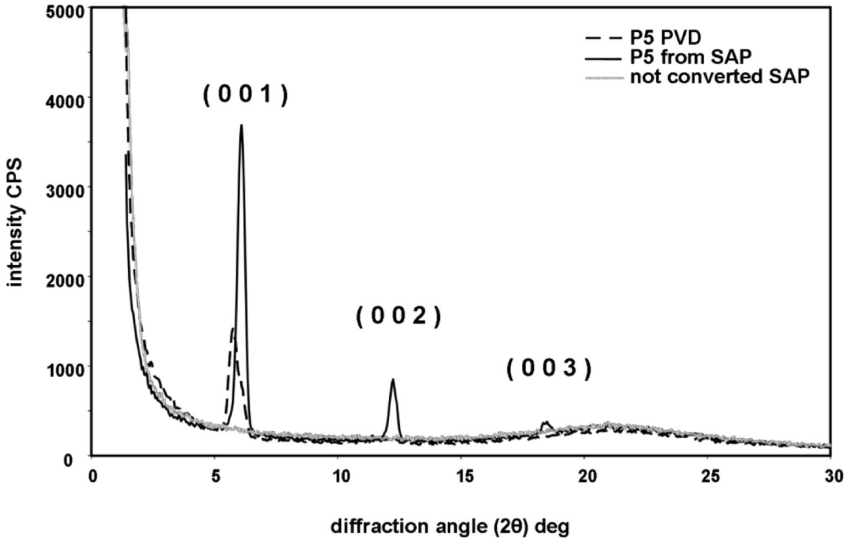

Figure 6. Out-of-plane WAXRD spectra of an unconverted SAP film (gray line); an SAP film thermally converted to pentacene (black continuous line); and a 40 nm thick vapor-deposited pentacene film (black dashed line).

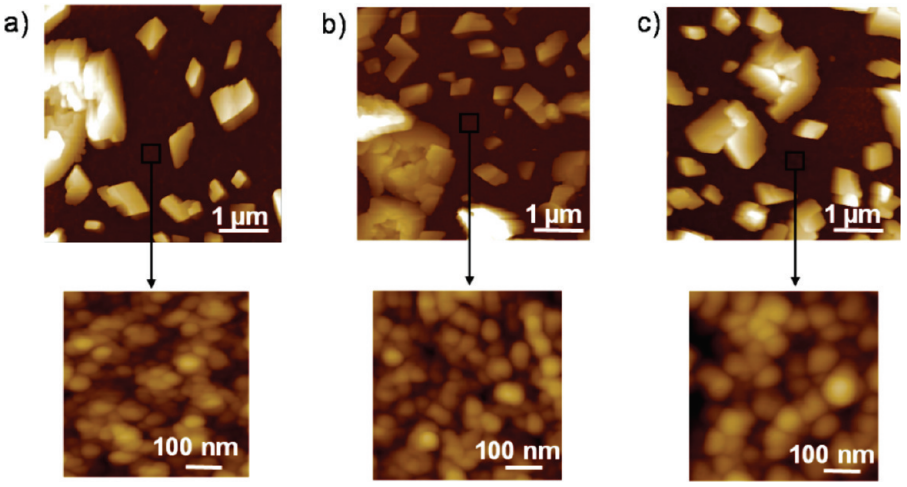

Figure 7. AFM topographic images of pentacene converted from SAP: a) in the channel; b) on a PEDOT:PSS electrode; and c) on gold; z scale: 500 nm. Bottom: expanded images in selected regions are reported to show the polycrystalline phase underlying/surrounding large islands; z scale: 50 nm.

PEDOT:PSS (Figure 7b), and on gold (Figure 7c). No obvious morphological differences are apparent in these films. To elucidate possible differences in the growth mode during SAP conversion and related surface and interfacial effects, thin films of SAP were grown by spin-coating dilute chloroform solutions on Si/SiO_2 substrates which supported either PVD Au or inkjet printed PEDOT:PSS electrodes. At first, 6 mg/mL solutions were used, and 40 nm thick SAP films were obtained by spin coating. On thermal treatment (120 °C, 30 min), pentacene islands up to 300 nm high with lateral sizes ranging from hundreds of nanometers to few micrometers are obtained. Interestingly, no significant differences are observed in the pentacene island morphological features at the edge perimeters of either the SiO_2/Au or SiO_2/PEDOT:PSS interface (Figures 8a,b below). This result indicates that the island formation is not critically affected by the surface chemistry, suggesting that growth occurs on the surface of an organic layer (converted/nonconverted SAP) in direct contact with the inorganic surfaces.

Note that enhanced electronic performance along with better pentacene morphological uniformity across the channel and the source/drain gold contacts was previously reported for SAP conversion in submicrometer channel devices.[55] Nevertheless, considering the OTFT channel lengths used here, a continuous charge carrier percolation pathway is obviously required through the polycrystalline film, since the large islands are randomly separated. Moreover, any field-induced carrier accumulation would be confined within the first layers of the semiconducting film, and, as reported above and in agreement with literature data,[39] the pentacene islands would more likely be on top of a thin polycrystalline layer.

To investigate in more detail the early growth stages of the thin organic layers in direct contact with the dielectric as well as with the S/D surfaces and interfaces, the polycrystalline pentacene phase was grown using a more dilute

(55) Tulevski, G. S.; Nuckolls, C.; Afzali, A.; Graham, T. O.; Kagan, C. R. *Appl. Phys. Lett.* **2006**, *89*, 183101.

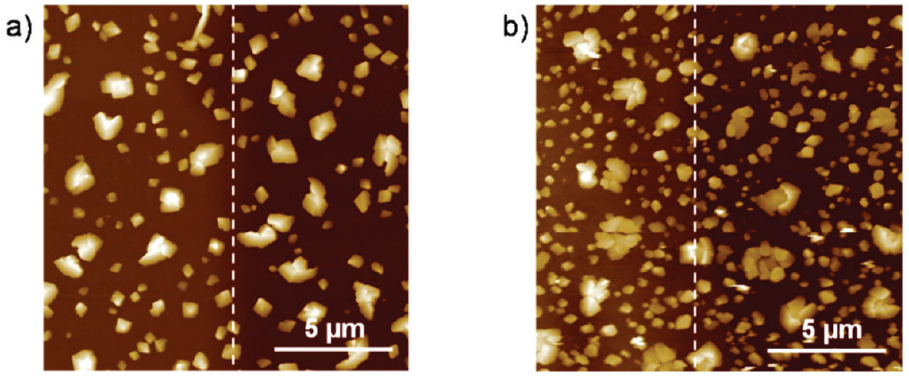

Figure 8. a) Island morphology of SAP films thermally converted to pentacene at the interfaces: a) Au/SiO_2; b) PEDOT:PSS/SiO_2; z scale: 500 nm.

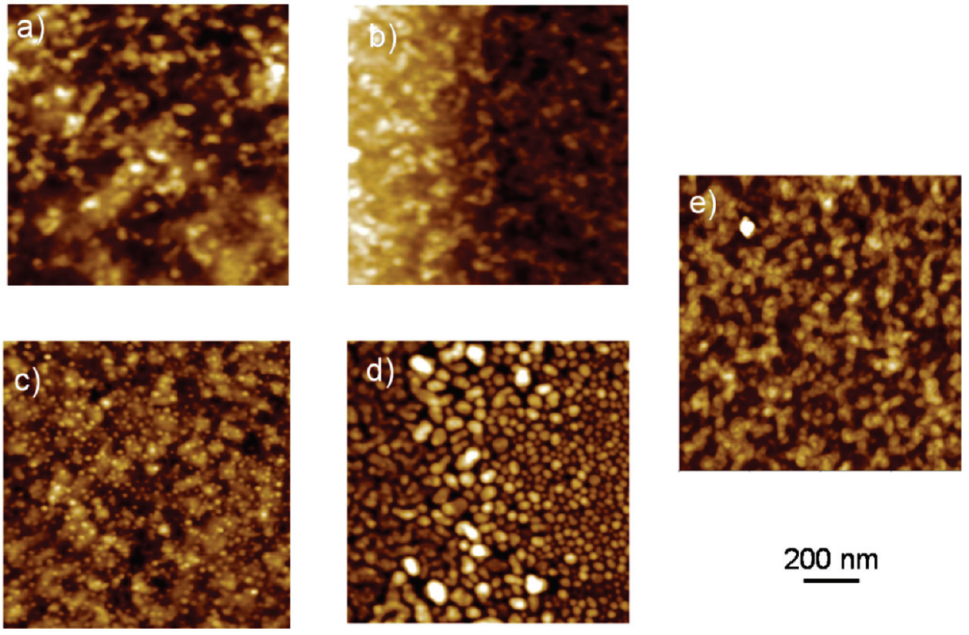

Figure 9. AFM images of the early growth stages of converted pentacene from SAP within different regions of device **1** and device **3**: a) on the PEDOT:PSS surface in device **1**; b) on the PEDOT:PSS/SiO_2 interface in device **1**; c) on the gold surface in device **3**; d) on the blurred region at the gold/SiO_2 edge in device **3**; and e) on the channels; z scale: 20 nm.

SAP chloroform solution (3 mg/mL), yielding film thicknesses of 7−10 nm (measured by AFM), and nucleating only small islands (hundreds of nms). To aid in comparing the effects of different electrode types on OTFT response, Figure 9 shows the organic layer film morphology grown on device types **1** and **3**. Note that there is no evidence for "layer-by-layer" growth of polycrystalline pentacene on SiO_2 (Figure 9e). However, the SAP-derived pentacene films on SiO_2 exhibit a "defect assisted" regime that induces the growth of the upper layers before completion of the first ones, leading to a disordered film structure.[40] Moreover, note that at this thickness (a few nms), hundreds of nm-scale pentacene islands are already observed, indicating that the islands and polycrystalline phase grow concurrently, beginning in the early growth stages.

In the case of device **1**, the thin pentacene layer exhibits a very similar morphology along with good morphological continuity and uniformity either across the channel or on the PEDOT:PSS electrodes and at their interface (Figures 9 a,b). In marked contrast, small disconnected mound-like particles of pentacene are visible on the Au electrode of device **3**. Moreover, at the edge region (Au/SiO_2 interface), there is no evidence of the pentacene layer, and the morphology of that region closely resembles that of free gold particles (Figures 9 c,d). A continuous pentacene polycrystalline phase is only observed several μms far from the Au edge within the channel. The above morphological features, including the discontinuity at the "blurred-edge",[54] emphasize the decisive effect of the gold surface in the assembly of the pentacene layer. This in turn explains the poor OTFT performance, arising from the poor pentacene crystallinity at the gold electrode edge and consequently, the limited charge injection into such devices (see devices **3** and **4** in Table 1).

In addition, the enhanced performance of device **4** versus device **3** can be explained by limited charge trapping[55] and/or a better morphology at the dielectric interface.[56,57] Note also that improved OTFT contact

(56) Yang, H.; Shin, T. J.; Ling, M. M.; Cho, K.; Ryu, C. Y.; Bao, Z. *J. Am. Chem. Soc.* **2005**, *127*, 11542.

resistances for a thermally converted SAP active phases have been reported using electron-beam deposited Au electrodes, for which mobilities ranging from ~0.2 to ~0.5 $cm^2 V^{-1} s^{-1}$ are obtained.[13,38] This latter growth technique should lead to better electrode pattern definition, limiting the blurred-edge region size.

4. Conclusions

One of the most important fabrication issues in the emerging field of plastic electronics concerns developing low-cost, large-scale solution deposition processes for organic molecules and polymers. In this respect, soluble pentacene precursors are among the best candidates for realizing high performance OTFTs. Due to the stochastic nature of organic film growth processes, one major challenge deals with controlling the organization of the charge accumulation layer at the dielectric and electrode interfaces. By employing the appropriate experimental parameters and inkjet printed organic electrodes, we are able to achieve microstructural continuity and uniformity of the pentacene polycrystalline phase across the device, and, in particular, across the dielectric/electrode interfacial region by thermal conversion of SAP. This situation is critical for achieving by means of a solution technology, performance comparable to that of polycrystalline silicon and/or vapor phase grown pentacene-based OTFTs.

Acknowledgment. This research was supported by the AFOSR (FA9550-08-1-0331), the NSF MRSEC program (DMR-0520513) at Northwestern University, the Italian MiUR ("PLAST_ICs, FART prot. MIUR DM 17767 art. 12lab"), and the University of Palermo.

Note Added after ASAP Publication. This article was published ASAP on January 10, 2011, with incorrect versions of Figures 1, 3, and 4. The corrected article was published ASAP on January 14, 2011.

(57) Musumeci, C.; Cascio, C.; Scandurra, A.; Indelli, G. F.; Bongiorno, C.; Ravesi, S.; Pignataro, B. *Surf. Sci.* **2008**, *602*, 993.